NUMERICAL METHODS FOR THE SIMULATION OF THE SETTLING OF FLOCCULATED SUSPENSIONS[†]

R. BÜRGER[a], S. EVJE[b], K. HVISTENDAHL KARLSEN[c,b,*], AND K.-A. LIE[d]

ABSTRACT. For one space dimension, the phenomenological theory of sedimentation of flocculated suspensions yields a model that consists of an initial-boundary value problem for a second order partial differential equation of mixed hyperbolic-parabolic type. Due to the mixed hyperbolic-parabolic nature of the model, its solutions may be discontinuous and difficulties arise if one tries to construct these solutions by classical numerical methods. In this paper we present and elaborate on numerical methods that can be used to correctly simulate this model, i.e., conservative methods satisfying a discrete entropy principle. Included in our discussion are finite difference methods and methods based on operator splitting. In particular, the operator splitting methods are used to simulate the settling of flocculated suspensions.

1. INTRODUCTION

Batch and continuous sedimentation processes are employed in a variety of industrial applications in which a solid-fluid suspension is separated into its solid and fluid components under the influence of gravity. Following the theory of mixtures of classical continuum mechanics, it is possible to derive a phenomenological theory for the settling of ideal and flocculated suspensions. The latter form a compressible sediment layer on the bottom of the sedimentation vessel, which motivates the expression 'sedimentation with compression'.

One of the first mathematically rigorous derivations of this theory was presented by Concha and Bustos [1], see also [2, 3]. This theory models a suspension as a mixture of two superimposed continuous media (the solids and the fluid), and starts from the usual local mass and linear momentum balances of both components. Introducing constitutive

---

Date: March 5, 1999.

Key words and phrases. Sedimentation, settling of flocculated suspensions, mixed hyperbolic-parabolic PDE, initial-boundary value problem, numerical simulation, finite difference method, operator splitting.

[†]Presented at the *United Engineering Foundation Conference on Solid-Liquid Separation Systems*, Kahuku, Oahu, Hawaii, USA, April 18–23, 1999.

[a]Institute of Mathematics A, University of Stuttgart, Pfaffenwaldring 57, D–70569 Stuttgart, Germany e-mail: `buerger@mathematik.uni-stuttgart.de`.

[b]RF-Rogaland Research, Thormølensgt. 55, N-5008 Bergen, Norway
e-mail: `Steinar.Evje@rf.no`.

[c]Department of Mathematics, University of Bergen, Johs. Brunsgt. 12, N–5008 Bergen, Norway
e-mail: `kenneth.karlsen@mi.uib.no`.

[d]Department of Informatics, University of Oslo, P.O. Box 1080, Blindern, N-0316 Oslo, Norway
e-mail: `kalie@ifi.uio.no`.

*Corresponding author.

assumptions, simplifying the balances as a result of an order-of-magnitude study, and restricting the motion to one space dimension yields an initial-boundary value problem for a second order partial differential equation (PDE) for the volumetric solids concentration ϕ. For a non-flocculated (ideal) suspension, the phenomenological model reduces to Kynch's well-known kinematic sedimentation model [4] and its extensions to continuous thickening [5, 6], which are described by a first order PDE.

An unusual feature of the governing equation of the phenomenological theory of sedimentation is its mixed hyperbolic-parabolic nature, where the mixed type nature corresponds to the interface between the compression zone, where the solid effective stress $\sigma_{\rm e}$ varies, and the hindered settling zone, where this quantity is assumed to be constant or to vanish. Solid effective stress can be transmitted when the solid flocs get into contact with each other and form a network, which is assumed to take place at a critical concentration value $\phi = \phi_{\rm c}$. Assuming that this quantity is a function of ϕ only, we consider constitutive equations $\sigma_{\rm e} = \sigma_{\rm e}(\phi)$ satisfying

$$\sigma_{\rm e}'(\phi) := \frac{d}{d\phi}\sigma_{\rm e}(\phi) \begin{cases} = 0 & \text{for } \phi \le \phi_{\rm c}, \\ > 0 & \text{for } \phi > \phi_{\rm c}. \end{cases} \tag{1}$$

Mathematically, the resulting governing equation behaves as a nonlinear parabolic PDE beneath the interface region and as a nonlinear hyperbolic one (corresponding to Kynch's theory) above the interface. The location of this interface is in general unknown beforehand, which introduces serious mathematical complications. In particular, as can be inferred from the well-established theory of conservation laws, solutions are in general discontinuous and have to be interpreted in some weak sense. Moreover, it turns out that such weak solutions are not uniquely determined by the data of the problem, and additional selection criteria, or entropy conditions, are needed to select the physically relevant one, the entropy weak solution, among possibly several weak solutions [7, 8, 9].

The nonlinear nature of the equation arising in the phenomenological theory rules out analytical solution techniques; consequently, this equation can be solved only numerically. This is in contrast to the possible construction of exact solutions in the Kynch theory of sedimentation by the method of characteristics [5, 10, 11].

The design of numerical methods for conservation laws, which could be applied to the Kynch model of sedimentation, has been subject of numerous papers that have been published in recent years. Several textbooks provide an excellent introduction to numerical methods for hyperbolic conservation laws, see, e.g., [12]–[15].

An appealing feature of the phenomenological sedimentation model is the fact that one single model equation can be employed both for the hindered settling process and for the consolidation of the sediment. Of course, the distinction between these processes is hidden in the mixed hyperbolic-parabolic type of this equation. The mathematical and numerical theory of such mixed type equations has yet to be raised to the same level of maturity as the equivalent theory of hyperbolic conservation laws. In fact, it is just until recently that papers [16]–[21] have appeared that consider numerical methods for this type of PDEs.

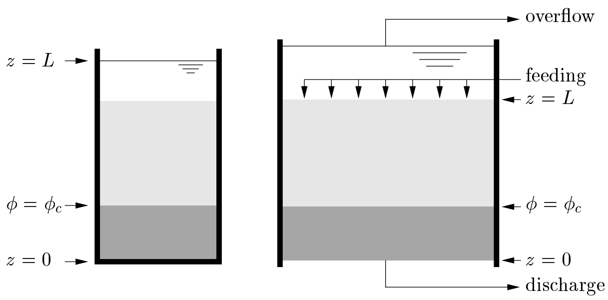

FIGURE 1. Ideal continuous thickener [26].

These works strongly emphasize the possibility to treat these equations without explicitly tracking the type-change interface or having to consider a free boundary value problem.

This view is clearly opposed to previous formulations of sedimentation-consolidation models by, e.g., Shodja and Feldkamp [23] and Stamatakis and Tien [24], who consider different equations for the hindered settling and for the consolidation zone and emphasize that a unified treatment of both zones by one equation would cause serious problems. It is the main objective of this paper to demonstrate that this is not the case and that the concept of hyperbolic-parabolic PDEs does not imply particular numerical problems as long as one follows a few general rules (see below).

The studies [16]–[21] were motivated by applications partially to sedimentation and partially to two-phase flow in oil reservoirs [22]. As pointed out in [19, 21], difficulties arise when attempting to solve numerically hyperbolic-parabolic PDEs using classical methods for parabolic PDEs. In particular, naive discretizations may fail to produce correct solutions, even in the limit as the discretization parameters tend to zero. As a general rule, one should use conservative methods for simulating the sedimentation model; namely, if conservative methods converge, then they do so to a (weak) solution of the model. Moreover, if conservative methods obey a discrete version of the entropy condition, they converge to the physically correct solution, see [16, 19, 20]. In this paper, we are concerned with conservative and entropy satisfying numerical methods for solving mixed hyperbolic-parabolic PDEs. In particular, numerical methods that can be used to simulate the batch and continuous sedimentation of flocculated suspensions are presented and demonstrated.

2. The Mathematical Model

We consider the settling of a flocculated suspension in an ideal continuous thickener (ICT) [6, 25], see Figure 1. An ICT is a cylindrical vessel showing no wall effects and in which all field variables are assumed to depend only on the height z and time t. At $z = L$, a surface feed and at $z = 0$, a surface discharge are provided for continuous operation. Included as a special case is a settling column for batch sedimentation, see Figure 1. In one space dimension, the phenomenological theory of sedimentation produces the following four field equations from the mass and linear momentum balances:

$$\frac{\partial \phi}{\partial t} + \frac{\partial}{\partial z}(\phi v_{\mathrm{s}}) = 0, \qquad \frac{\partial q}{\partial z} = 0 \quad \text{or} \quad q = q(t), \tag{2}$$

$$\frac{\partial \sigma_{\mathrm{e}}}{\partial z} = -\Delta\varrho\phi g - \frac{\alpha(\phi) v_{\mathrm{r}}}{1-\phi}, \qquad \frac{\partial p_{\mathrm{e}}}{\partial z} = \frac{\alpha(\phi) v_{\mathrm{r}}}{1-\phi}. \tag{3}$$

Across discontinuities these field equations are replaced by appropriate Rankine-Hugoniot jump conditions. We refer to [2] and Bürger's contribution to this special issue [27] for details on the derivation of the phenomenological theory. In (2) and (3), $q = \phi v_{\mathrm{s}} + (1-\phi) v_{\mathrm{f}}$ is the volume average velocity of the mixture, v_{s} and v_{f} are the solid and fluid component velocities, $\Delta\varrho = \varrho_{\mathrm{s}} - \varrho_{\mathrm{f}}$, ϱ_{s} and ϱ_{f} are the solids and fluid densities, g is the acceleration of gravity, p_{e} the excess pore pressure, and $\alpha(\phi)$ a scalar function relating the solid-fluid interaction force per unit mass to the relative solid-fluid velocity $v_{\mathrm{r}} = v_{\mathrm{s}} - v_{\mathrm{f}}$. The material specific behaviour of the suspension is described only by the functions α and σ_{e}. One can use the first part of (3) and the definition of q to deduce that the solids volume flux per unit area ϕv_{s} takes the from

$$\phi v_{\mathrm{s}} = q\phi + \phi(1-\phi) v_{\mathrm{r}} = q\phi - \Delta\varrho g \frac{\phi^2(1-\phi)^2}{\alpha(\phi)} \Big(1 + \frac{\sigma_{\mathrm{e}}'(\phi)}{\Delta\varrho g \phi} \frac{\partial \phi}{\partial z}\Big). \tag{4}$$

We assume that $\sigma_{\mathrm{e}}(\phi)$ satisfies condition (1). Introducing the Kynch batch flux density function

$$f_{\mathrm{bk}}(\phi) = -\frac{\Delta\varrho g \phi^2 (1-\phi)^2}{\alpha(\phi)}$$

and $f(\phi, t) = q(t)\phi + f_{\mathrm{bk}}(\phi)$ and inserting (4) into the first part of (2), the continuity equation for $\phi(z,t)$ reads

$$\frac{\partial \phi}{\partial t} + \frac{\partial}{\partial z} f(\phi, t) = \frac{\partial}{\partial z}\Big(-f_{\mathrm{bk}}(\phi) \frac{\sigma_{\mathrm{e}}'(\phi)}{\Delta\varrho g \phi} \frac{\partial \phi}{\partial z}\Big). \tag{5}$$

We assume $q(t) \leq 0$ for $t \in (0,T)$, $f_{\mathrm{bk}}(0) = f_{\mathrm{bk}}(\phi_{\max}) = 0$, and $f_{\mathrm{bk}}(\phi) < 0$ for $\phi \in (0, \phi_{\max})$, where $0 < \phi_{\max} \leq 1$ is the maximum solids concentration. For definiteness, we set $f_{\mathrm{bk}}(\phi) = 0$ for $\phi < 0$ and $\phi > \phi_{\max}$. Equation (5) is a second order parabolic equation which for $\phi < \phi_{\mathrm{c}}$ degenerates into the hyperbolic equation of Kynch's theory of continuous thickening. Introducing the diffusion function

$$a(\phi) = -\frac{f_{\mathrm{bk}}(\phi)\sigma_{\mathrm{e}}'(\phi)}{\Delta\varrho g \phi}, \tag{6}$$

we see that $a(\phi) = 0$ for $\phi < \phi_{\mathrm{c}}$ and $\phi \geq \phi_{\max}$ and $a(\phi) > 0$ for $\phi_{\mathrm{c}} \leq \phi < \phi_{\max}$. Hence, the mixed hyperbolic-parabolic nature of the PDE (5) becomes evident. The location of the type change is unknown beforehand.

We assume that for $t = 0$, an initial concentration profile $\phi_0(z)$ is given, and that at $z = L$, a concentration value $\phi_L(t)$ is prescribed for $0 \leq t \leq T$. The discharge control at $z = 0$ corresponds to reducing the solids volume flux across $z = 0$ to the convective part $q(t)\phi(0,t)$. Summing up, the volumetric solids concentration $\phi(z,t)$ in the thickener satisfies the following initial-boundary value problem (IBVP):

$$\frac{\partial \phi}{\partial t} + \frac{\partial}{\partial z} f(\phi, t) = \frac{\partial}{\partial z}\Big(a(\phi)\frac{\partial \phi}{\partial z}\Big), \qquad (z,t) \in \Pi_T = (0,L) \times (0,T), \tag{7}$$

$$\phi(z,0) = \phi_0(z), \qquad z \in (0,L), \tag{8}$$

$$f_{\mathrm{bk}}(\phi) - a(\phi)\frac{\partial \phi}{\partial z}\Big|_{z=0} = 0 \quad \text{and} \quad \phi(L,t) = \phi_L(t), \qquad t \in (0,T). \tag{9}$$

By using the second part of (3), the excess pore pressure p_{e} can be calculated after the concentration $\phi(z,t)$ has been calculated and is therefore not included into the formulation of the initial-boundary value problem.

It is well known that solutions of mixed hyperbolic-parabolic problems will in general become discontinuous in finite time, even if the initial and boundary data are infinitely smooth. It thus becomes necessary to consider weak solutions. However, for given initial and boundary data, a plenitude of weak solutions may exist. To ensure uniqueness, we therefore consider weak solutions satisfying an additional condition called the entropy condition (the so-called generalized solutions). The IBVP (7)–(9) was analysed within the framework of generalized solutions by Bürger and Wendland [8, 9]. In [9], existence and uniqueness of generalized solutions were established under certain smoothness and compatibility assumptions on the data and the coefficients of the problem. An improved analysis can be found in Bürger, Evje, and Karlsen [7], where, for example, the smoothness assumptions on the coefficients have been relaxed. In particular, $a(\phi)$ is allowed to be discontinuous, which is of interest since many empirical approaches for the effective solid stress σ_{e} stipulate a jump at $\phi = \phi_{\mathrm{c}}$, see [28, 29].

Moreover, it turns out that the propagation velocity of the concentration discontinuity at the sediment-suspension interface is no longer given by the common Rankine-Hugoniot conditions in terms adjacent concentration values only; rather than that the limit of the partial derivative of $A(\phi)$ with respect to z is involved. In most circumstances, this makes the propagation speed of this interface unpredictable a priori, in contrast to what is known for the Kynch model, where the Rankine-Hugoniot condition has been exploited to formulate a control model [30] for continuous sedimentation.

3. Finite Difference Methods

This section provides the necessary background for the development and application of numerical methods for mixed hyperbolic-parabolic problems. Our prime objective is to present a few working difference methods in a simple setting so as to ease the development of numerical methods for the sedimentation model in the next section. The finite difference methods described below can, however, be easily modified to solve the full sedimentation model. To focus on the main ideas, we consider here only the simplified problem

$$\frac{\partial \phi}{\partial t} + \frac{\partial}{\partial z} f(\phi) = \frac{\partial}{\partial z}\Big(a(\phi)\frac{\partial \phi}{\partial z}\Big), \qquad \phi(z,0) = \phi_0(z), \tag{10}$$

where $\phi = \phi(x,t)$ is the unknown function and $f = f(\phi), a = a(\phi) \geq 0, \phi_0 = \phi_0(z)$ are given, smooth functions (not necessarily the ones given in §2). It is not difficult to modify the difference methods below so that time dependent fluxes and boundary conditions can be taken into account. The material presented here is based on the series of papers by Evje and Karlsen [17, 18, 19, 21].

Selecting a mesh size $\Delta z > 0$, a time step $\Delta t > 0$, and an integer N so that $N\Delta t = T$, the value of the difference approximation at $(z_j, t_n) = (j\Delta z, n\Delta t)$ will be denoted by ϕ_j^n. There are special difficulties associated with solving mixed type problems which must be dealt with in developing numerical methods. First of all, as was pointed out in [19, 21], numerical methods based on naive finite difference formulation of the diffusion term may be adequate for smooth solutions but can give wrong results when discontinuities are present. The following example demonstrates the problem.

Example 3.1 (Conservative vs Non-Conservative Discretization). *Since the focus will be on the discretization of the diffusion term, we consider here only the pure "diffusion" equation*

$$\frac{\partial \phi}{\partial t} = \frac{\partial}{\partial z}\Big(a(\phi)\frac{\partial \phi}{\partial z}\Big) = \frac{\partial^2}{\partial z^2}A(\phi), \qquad A(\phi) = \int_0^\phi a(\xi)\, d\xi. \tag{11}$$

A natural finite difference formulation of (11) *is*

$$\frac{\phi_j^{n+1} - \phi_j^n}{\Delta t} = \frac{a(\phi_{j+1/2}^n)\frac{\phi_{j+1}^n - \phi_j^n}{\Delta z} - a(\phi_{j-1/2}^n)\frac{\phi_j^n - \phi_{j-1}^n}{\Delta z}}{\Delta z}, \tag{12}$$

where $\phi_{j+1/2}^n = (\phi_j^n + \phi_{j+1}^n)/2$. *We refer to* (12) *as a non-conservative discretization of* (11). *On the other hand, a different but still natural finite difference formulation of* (11) *is*

$$\frac{\phi_j^{n+1} - \phi_j^n}{\Delta t} = \frac{A(\phi_{j-1}^n) - 2A(\phi_j^n) + A(\phi_{j+1}^n)}{(\Delta z)^2}. \tag{13}$$

We refer to (13) *as a conservative discretization of* (11). *It can be easily be shown that* (12) *and* (13) *both are stable and convergent under the stability condition (see* [19]*)*

$$2\max_\phi |a(\phi)| \frac{\Delta t}{(\Delta z)^2} \leq 1. \tag{14}$$

Nevertheless, we next demonstrate that (12) *produces wrong discontinuous solutions. To this end, consider* (11) *with an initial condition* $\phi_0(z)$ *as shown in Figure 2 and a diffusion function* $a(\phi)$ *given by*

$$a(\phi) = \begin{cases} 0, & \text{for } 0 \leq \phi < 2, \\ 1, & \text{for } 2 \leq \phi \leq 3, \end{cases} \tag{15}$$

Note that since $a(\cdot) \geq 0$ *the exact solution is discontinuous (at two points). In Figure 2, we have plotted the approximate solutions calculated by* (12) *and* (13) *at two different times. We have used a fine space step* $\Delta z = 0.001$ *and a time step* Δt *satisfying* (14). *Clearly, the two methods produce two different solutions. In* [19], *it is mathematically* *proved that (13) is the correct discretization. Finally, we mention that in the parabolic case $a(\cdot) > 0$ where the solution is smooth, the two methods (12) and (13) produce the same solution. In other words, the phenomenon displayed in Figure 2 is a consequence of the mixed hyperbolic-parabolic nature of the governing PDE.*

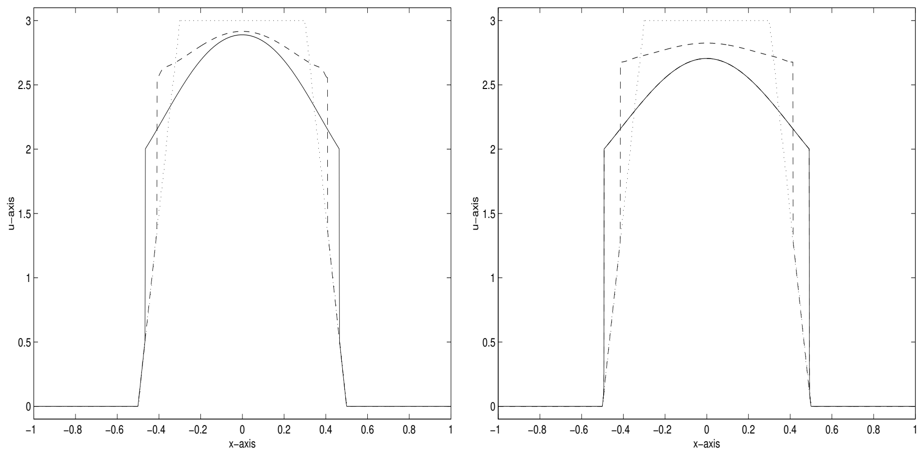

FIGURE 2. Solutions produced by the non-conservative method (12) (dashed) and the conservative method (13) (solid) at times $T = 0.05$ (left) and $T = 0.1$ (right). The initial condition is shown as dotted. Note that the the non-conservative method produces wrong solutions!

In view of Example 3.1, it can be tempting to approximate the solution of the convection-diffusion problem (10) by the central differencing method

$$\frac{\phi_j^{n+1} - \phi_j^n}{\Delta t} + \frac{f(\phi_{j+1}^n) - f(\phi_{j-1}^n)}{2\Delta z} = \frac{A(\phi_{j-1}^n) - 2A(\phi_j^n) + A(\phi_{j+1}^n)}{(\Delta z)^2}.$$

Although this works very well in the strictly parabolic case $a(\cdot) > 0$, this discretization is not suitable for the mixed hyperbolic-parabolic case $a(\cdot) \geq 0$. In particular, the central approximation of the convection flux f will produce non-physical oscillations in the vicinity of high gradients of the solution. In turns out that it is preferable to use upwind differencing, i.e., a difference method of the form

$$\frac{\phi_j^{n+1} - \phi_j^n}{\Delta t} + \frac{F(\phi_j^n, \phi_{j+1}^n) - F(\phi_{j-1}^n, \phi_j^n)}{\Delta z} = \frac{A(\phi_{j-1}^n) - 2A(\phi_j^n) + A(\phi_{j+1}^n)}{(\Delta z)^2}, \tag{16}$$

where F is the upwind flux. For a monotone flux function f, the upwind flux is defined by $F(\phi_j^n, \phi_{j+1}^n) = f(\phi_j^n)$ if $f' > 0$ and $F(\phi_j^n, \phi_{j+1}^n) = f(\phi_{j+1}^n)$ if $f' < 0$. More generally, for a non-monotone flux function f, one needs the generalised upwind flux of Engquist and Osher, see [19]. The upwind method (16) is stable provided the following stability condition holds:

$$\max_{\phi} |f'(\phi)| \frac{\Delta t}{\Delta z} + 2 \max_{\phi} |a(\phi)| \frac{\Delta t}{(\Delta z)^2} \leq 1.$$

It appears that upwind differencing stabilizes profiles which are liable to undergo sudden changes, i.e., discontinuities and other large gradient profiles. Therefore upwind differencing is perfectly suited to the treatment of discontinuities (and thus of the sedimentation model). In fact, it can be shown mathematically that the upwind method (16) satisfies a discrete entropy condition and that it converges in a non-oscillatory manner to the unique generalized solution of (10), see [19] for details. The same results actually hold for all monotone difference methods (the upwind method is a monotone method).

The upwind method (and all other monotone methods) are at most first order accurate, giving poor accuracy in smooth regions. To overcome these problems, Evje and Karlsen [17] used the generalized MUSCL (variable extrapolation) idea to formally upgrade the upwind method (16) to second order accuracy. The MUSCL approach is based on a piecewise linear reconstruction of the cell averages at each time level to increase the resolution. This approach is today employed in many numerical methods for hyperbolic conservation laws, see [12]–[15]. Although more difficult than in the monotone case, it can be shown that also the second order method satisfies a discrete entropy condition and that it converges to the unique generalized solution of the problem, see [17] for details. Let us give an example of a second order upwind method. To this end, we introduce the extrapolated values

$$\phi_j^{\mathrm{L}} = \phi_j^n - \frac{\Delta z}{2} s_j^n, \qquad \phi_j^{\mathrm{R}} = \phi_j^n + \frac{\Delta z}{2} s_j^n,$$

where s_j^n is some slope that satisfies $s_j^n = \frac{\partial}{\partial z}\phi(z_j, t_n) + \mathcal{O}(\Delta z)$ and certain monotonicity constraints to ensure that the overall approximation is non-oscillatory. The second order method is identified by the choice of a limiter function $s(\cdot,\cdot)$ that defines the slopes;

$$s_j^n = s\big(\tfrac{\phi_j^n - \phi_{j-1}^n}{\Delta z}, \tfrac{\phi_{j+1}^n - \phi_j}{\Delta z}\big),$$

and is usually constrained by $\min(a,b) \le s(a,b) \le \max(a,b)$. There exists a variety of possible limiters $s(\cdot,\cdot)$, see Example 3.2 below and, e.g., [12]–[15]. The second order upwind method now takes the form

$$\frac{\phi_j^{n+1} - \phi_j^n}{\Delta t} + \frac{F(\phi_j^{\mathrm{R}}, \phi_{j+1}^{\mathrm{L}}) - F(\phi_{j-1}^{\mathrm{R}}, \phi_j^{\mathrm{L}})}{\Delta z} = \frac{A(\phi_{j-1}^n) - 2A(\phi_j^n) + A(\phi_{j+1}^n)}{(\Delta z)^2}. \tag{17}$$

We note that all three-point monotone methods can be upgraded to second order accuracy using the generalized MUSCL approach, see [17]. In the following example we demonstrate the difference between a first and second order upwind method:

Example 3.2 (First vs Second Order Upwind Methods). *In Figure 3 we display the solutions obtained by the first and second order upwind methods* (16) *and* (17)*, respectively. In the second order method, we have used the so-called minmod limiter (see, e.g.,* [12]–[15]*)*

$$s(a,b) = \tfrac{1}{2}\big[\mathrm{sgn}(a) + \mathrm{sgn}(b)\big] \min\big(|a|, |b|\big).$$

We have calculated the approximate solution at time $T = 0.2$ and on a rather coarse grid, $\Delta z = 1/15$. We have used the Burgers flux $f(\phi) = \phi^2/2$ and the diffusion flux $a(\phi)$ is given in (15)*. The initial condition $\phi_0(z)$ is shown in Figure 3. This plot clearly demonstrates* *how the approximation of the smooth parts of the solution is improved by using the second order method.*

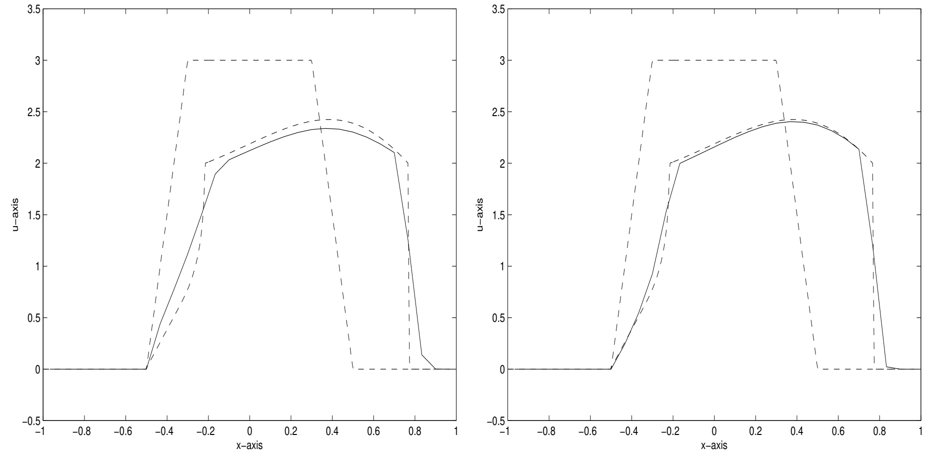

FIGURE 3. Solutions produced by the first order (left) and second order (right) upwind methods (16) and (17), respectively. Initial condition (box like) and exact solution are both shown as dashed. Approximate solutions are shown as solid.

4. Operator Splitting Methods

There are essentially two ways of constructing methods for solving convection-diffusion problems such as (7)–(9). One approach attempts to preserve some coupling between the two processes involved (convection and diffusion). The finite difference methods considered in the previous section try to follow this approach. Another approach is to split the convection-diffusion problem into a convection problem and a diffusion problem. The split problems are then solved sequentially to approximate the exact solution of the model. The intermediate solutions resulting from the use of operator splitting are numerical artifacts and have no physical equivalence. In the physical problem all the transport processes, convection and diffusion, take place simultaneously. However, in the splitting methods these processes are imposed on the initial condition sequentially. The main attraction of splitting methods lies, of course, in the fact that one can employ the optimal existing methods for each subproblem.

In this section, we devise some accurate and efficient splitting methods for simulating the sedimentation model (7)–(9). The splitting methods presented here are similar to the splitting methods that have been used over the years to simulate multi-phase flow in oil reservoirs. We refer to the lecture notes by Espedal and Karlsen [22] for an overview of this activity and an introduction to operator splitting methods in general. The construction of operator splitting methods is, of course, not unique, neither with respect to the choice of splitting nor the choice of numerical methods for the resulting split problems. In what follows, we present only two possible splitting methods. More sophisticated methods, so-called corrected operator splitting methods, are described in Karlsen *et al.* [31, 32, 33, 22].

4.1. **Operator Splitting by Front Tracking.** We shall here outline a variant of the operator splitting method used by Evje and Karlsen [20]. As the boundary conditions (9) are defined for the unsplit PDE (7), it is necessary to determine appropriate boundary conditions for the split equations. In the splitting methods considered in this paper, the boundary conditions defined by the physical problem have been directly applied to one of the split equations. As the simulation characteristics of the methods are demonstrated for boundary conditions that are more or less independent of time, the presented results are good. However, this conclusion may not hold if the boundary condition are highly time dependent. The treatment of boundary conditions in operator splitting methods is investigated thoroughly in Bürger, Evje, and Karlsen [16].

The operator splitting used in this section splits the original IBVP (7)–(9) into the purely hyperbolic IBVP problem

$$\begin{cases} \frac{\partial v}{\partial t} + \frac{\partial}{\partial z} f(v,t) = 0, & (z,t) \in \Pi_T, \\ v(z,0) = v_0(z), & z \in (0,L), \\ v(L,t) = \phi_L(t), & t \in (0,T). \end{cases} \tag{18}$$

and the second order IBVP problem

$$\begin{cases} \frac{\partial w}{\partial t} = \frac{\partial}{\partial z}\big(a(w)\frac{\partial w}{\partial z}\big), & (z,t) \in \Pi_T = (0,L)\times(0,T), \\ w(z,0) = w_0(z), & z \in (0,L), \\ f_{\mathrm{bk}}(w) - a(w)\frac{\partial w}{\partial z}\big|_{z=0} = 0, \quad w(L,t) = \phi_L(t), & t \in (0,T). \end{cases} \tag{19}$$

Note that no boundary condition is specified at $z = 0$ in (18). This corresponds to an outflow condition where waves leave the domain without any form of reflection. For simplicity of notation, we shall denote the effect of the consecutive solution steps by 'solution operators'. To be more precise, we let $\mathcal{S}^f(t)$ denote the solution operator taking the initial data $v_0(z)$ to the generalized solution at time t of (18), and write $v(z,t) = \mathcal{S}^f(t)v_0(z)$ for this solution. Similarly, we let $\mathcal{H}(t)$ denote the operator taking the initial data $w_0(z)$ to the generalized solution at time t of (19), and write $w(z,t) = \mathcal{H}(t)w_0(z)$ for this solution.

Now choosing a splitting step $\Delta t > 0$ and an integer N such that $N\Delta t = T$, we define the splitting approximation $\phi_{\Delta t}$ by

$$\phi_{\Delta t}(z,(n+1)\Delta t) := \Big[\mathcal{H}(\Delta t)\circ \mathcal{S}^f(\Delta t)\Big]\phi_{\Delta t}(z,n\Delta t), \tag{20}$$

where $n = 0,\dots,N-1$ and $\phi_{\Delta t}(z,0) = \phi_0(z)$. A mathematical analysis of this splitting procedure can be found in Evje and Karlsen [20] and in Bürger, Evje, and Karlsen [16]. In particular, these authors have demonstrated that (20) satisfies a discrete entropy condition and thus approaches the unique generalized solution as Δt goes to zero. Consequently, (20) can be used as a basis for the construction of numerical methods.

Note that so far we have assumed that the operators $\mathcal{S}^f(t)$ and $\mathcal{H}(t)$ determine exact solutions to their respective split problems and that discretization has been performed with respect to time only. In applications, the exact solution operators $\mathcal{S}^f(t)$ and $\mathcal{H}(t)$ are replaced by appropriate numerical approximations which involve discretization also with respect to space. For the hyperbolic problem (18), one can choose from a diversity of methods described in the books [12]–[15] and [34]. For the second order problem (19), one can also choose from a large collection of finite difference or element methods, although one should bear in mind the problem pointed out in Example 3.1 when choosing a method.

In the particular numerical realization of (20) implemented here, we have used the conservative central method (13) to solve the second order problem (19). Assuming that the space step $\Delta z > 0$ is provided by the user, a local time step $\tau = \Delta t / N_\tau$ ($N_\tau \geq 1$ an integer) is chosen for the central method so that the stability condition

$$\frac{2\tau}{(\Delta z)^2} \max_w |a(w)| \leq 1 \tag{21}$$

is satisfied. The central difference approximation is then calculated up to time $t = \Delta t$ (the splitting step) using τ as the time step. The boundary condition at $z = 0$ is written $f(w) - A(w)_z = 0$ and discretized explicitly by central differences.

To construct approximate solutions of the hyperbolic problem (18) we use front tracking as introduced by Dafermos [35]. Suppose that the initial function $v_0(z)$ is piecewise constant. Then the local solution of the conservation law

$$\frac{\partial v}{\partial t} + \frac{\partial}{\partial z} f(v), \qquad v(z,0) = v_0(z)$$

can be constructed by a superposition of solutions of Riemann problems, i.e., solutions of the conservation law with initial data consisting of two constant states separated by a simple discontinuity. If the flux is piecewise linear, each Riemann solution consists exclusively of constant states separated by shocks. When waves from neighbouring Riemann problems interact, the interaction will only involve constant states and therefore lead to new Riemann problems and the construction can be continued forward in time. Thus, the construction consists of solving Riemann problems and tracking straight-line discontinuities. In the general case, the initial function is approximated by a step function and the flux by a piecewise linear function. This way rarefaction waves are approximated by a sequence of small shocks. Variants of the method have been used by many authors, see, e.g., Holden and Risebro [34] or Lie [36] for more references. In particular, Holden, Holden, and Høegh–Krohn [37, 38] proved that the construction is well-defined and terminate in a finite number of steps, even for non-convex flux functions, given a finite number of constant states in $v_0(z)$. Front tracking was later reformulated for hyperbolic systems by Risebro [39] and is in use both as a mathematical tool and as a numerical method (see [34, 36]).

The front tracking method can easily be extended to equations with variable coefficients, see Lie [40]. Here we will use a variant of this approach. Due to the special form of the flux function, $f(v,t) = q(t)v + f_{\mathrm{bk}}(v)$, the Riemann solution can be constructed using only the Kynch batch flux $f_{\mathrm{bk}}(v)$. The discontinuities in the solution then satisfy the following differential equation $z'(t) = q(t) + s_{\mathrm{bk}}$, where s_{bk} denotes the Rankine–Hugoniot shock speed for the Kynch batch flux function f_{bk}. If $q(t)$ is simple, the differential equation for $z(t)$ can be solved exactly. If not, $q(t)$ is approximated by, e.g., a piecewise linear function and then solved exactly. The boundary conditions are also easy to include. The function $\phi_L(t)$ is approximated by a step function, and a new Riemann problem is solved for each step or when a wave interacts with the boundary. In the Kynch theory the boundary condition at $z = 0$ becomes $f_{\rm bk}(v) = 0$. This zero-flux condition is treated by solving a Riemann problem with a fictitious left state v_L satisfying $f_{\rm bk}(v_L) = 0$. In both cases, only shocks propagating into the domain are kept in each Riemann solution. See Karlsen, Lie, and Risebro [41] for more details.

Finally, we note that the numerical realization of (20) based on front tracking constitutes a conservative and entropy satisfying numerical method, see [20].

4.2. **Operator Splitting by Finite Differencing.** We shall in this section outline the operator splitting method used by Bürger and Wendland [42] and by Bustos *et al.* [2], which is slightly different from the method described in §4.1. This method splits the original IBVP (7)–(9) into the second order problem

$$\begin{cases} \frac{\partial w}{\partial t} = \frac{\partial}{\partial z}\big(a(w)\frac{\partial w}{\partial z}\big), & (z,t) \in \Pi_T = (0,L) \times (0,T), \\ w(z,0) = w_0(z), & z \in (0,L), \end{cases} \tag{22}$$

the linear convection problem

$$\begin{cases} \frac{\partial u}{\partial t} + q(t)\frac{\partial u}{\partial z} = 0, & (z,t) \in \Pi_T, \\ u(z,0) = u_0(z), & z \in (0,L), \end{cases} \tag{23}$$

and the nonlinear hyperbolic IBVP problem

$$\begin{cases} \frac{\partial v}{\partial t} + \frac{\partial}{\partial z} f_{\rm bk}(v) = 0, & (z,t) \in \Pi_T, \\ v(z,0) = v_0(z), & z \in (0,L) \\ f_{\rm bk}(v) - a(v)\frac{\partial v}{\partial z}\Big|_{z=0} = 0, \quad v(L,t) = \phi_L(t), & t \in (0,T). \end{cases} \tag{24}$$

If we denote by $\mathcal{H}(\Delta t)$, $\mathcal{S}^q(t)$, and $\mathcal{S}^{f_{\rm bk}}(t)$ the solution operators of (23), (24), (22), respectively, the splitting approximation $\phi_{\Delta t}$ can be compactly defined by

$$\phi_{\Delta t}(z,(n+1)\Delta t) = \Big[\mathcal{S}^{f_{\rm bk}}(\Delta t) \circ \mathcal{S}^q(\Delta t) \circ \mathcal{H}(\Delta t)\Big]\phi_{\Delta t}(z, n\Delta t), \tag{25}$$

where $n = 0, \dots, N-1$ and $\phi_{\Delta t}(z,0) = \phi_0(z)$. Note that the ordering of the operators in (25) is different from the ordering used in (20). Also, the boundary conditions are taken into account only in the nonlinear hyperbolic step (24), which is different from the boundary treatment in the two-step splitting described in §4.1. The splitting (25) is analysed mathematically in [20, 16].

In the particular numerical realization of (25) implemented here, we have used the conservative central method (13) to solve the second order problem (22), a first order upwind method to solve the linear convection problem (23), and, finally, a variant of Nessyahu and Tadmor's method [43] for solving the nonlinear convection problem (24). We recall that the Nessyahu and Tadmor method is a high-resolution conservative method which satisfies a discrete entropy principle. Consequently, the implemented splitting method is

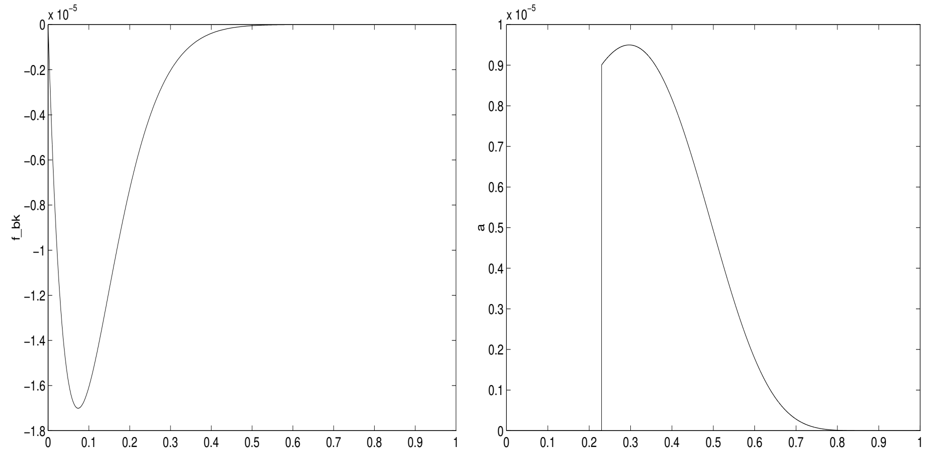

FIGURE 4. The Kynch batch flux density function $f_{\mathrm{bk}}(\phi)$ (left) and the diffusion function $a(\phi)$ (right) used in §5.1 and §5.2.

conservative and entropy satisfying, see [16]. We do not explicitly state the formulas for the methods used to solve the split problems. These can, however, be found in [2, 42].

5. Simulation of Sedimentation with Compression

We now demonstrate the operator splitting methods described in the previous section by applying them to three problems related to the simulation of sedimentation with compression. These problems are adopted from Bürger *et al.* [44].

5.1. **Batch settling of a flocculated suspension.** We consider a settling column of height $L = 6$ [m] closed at the bottom ($q \equiv 0$) and without feed ($\phi_L = 0$), filled with a flocculated suspension of the initially homogeneous concentration $\phi_0 = 0.123$. We use a Kynch batch flux density function of the well known Richardson and Zaki type [45],

$$f_{\mathrm{bk}}(\phi) = -6.05 \times 10^{-4}\phi(1-\phi)^{12.59}\ [\mathrm{m/s}],$$

and the solid effective stress function

$$\sigma_{\mathrm{e}}(\phi) = \begin{cases} 0, & \phi \leq \phi_{\mathrm{c}} = 0.23, \\ 5.35 \times \exp(17.9\phi)\ [\mathrm{N/m^2}], & \phi > \phi_{\mathrm{c}} \end{cases}$$

determined by Becker [46] based on experimental measurements on Chilean copper ore tailings. Note that this choice σ_{e} leads to a diffusion function $a(\phi)$ that is discontinuous, see (6). Furthermore, we use the parameters $\Delta\varrho = \varrho_{\mathrm{s}} - \varrho_{\mathrm{f}} = 1500$ [kg/m^3] and $g = 9.81$ [m/s^2]. The flux and the diffusion functions are plotted in Figure 4. An analysis of the sedimentation model with discontinuous diffusion functions is presented in [7].

Figure 5 shows the settling plot and some selected concentration profiles for sedimentation up to final time $T = 345600$ [s] ≈ 96 [h] computed by operator splitting (20). The solution is computed on a grid with 300 cells using 3000 time steps. The overall quality of the operator splitting solution is very good (as has been documented in previous

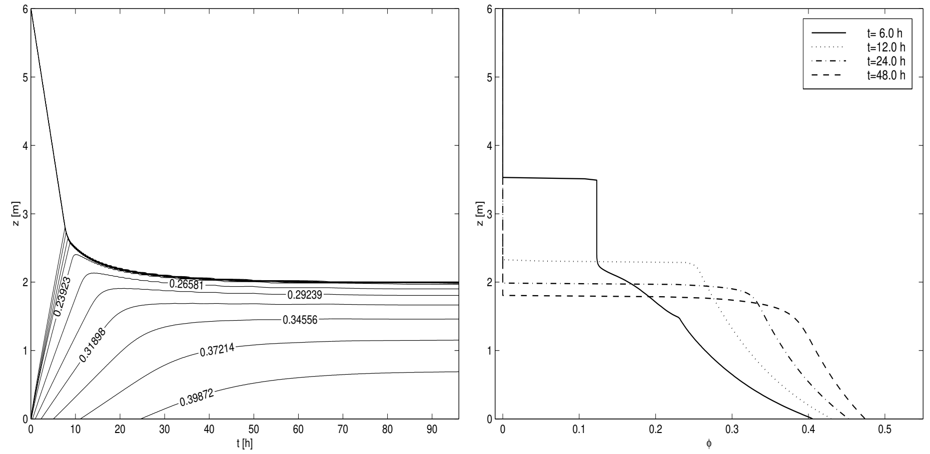

FIGURE 5. Settling plot (left) and concentration profiles (right) for batch settling of a flocculated suspension simulated by operator splitting (20).

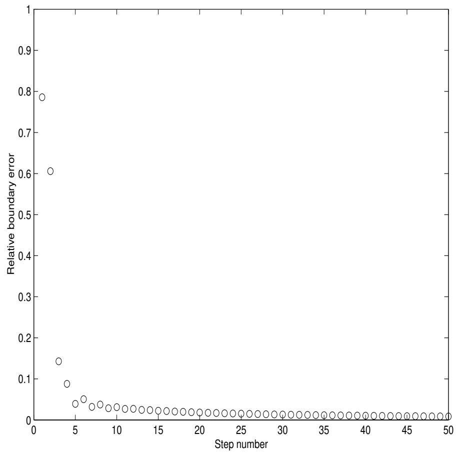

FIGURE 6. Error measured at the boundary $z = 0$ in the first 50 splitting steps (normalized by $\max|f|$) using the operator splitting defined in (20).

studies [32, 33]). However, it might seem strange that the crude splitting of the boundary condition at $z = 0$ gives no visual effect on the solution. But if we compute the error at the boundary (boundary residual), we see that it decays exponentially with time (see Figure 6). Moreover, the lack of mass conservation is at most 0.12%.

To make the difference to Kynch's theory apparent, we also present a computation performed with $\sigma_e \equiv 0$, see Figure 7. Notice especially two features of the solution; the suspension-sediment interface and the much higher concentration close to the boundary.

5.2. **Filling and emptying of a continuous thickener.** We consider the same parameters as before and assume that the ICT is initially full of water, $\phi_0 \equiv 0$. The average flow

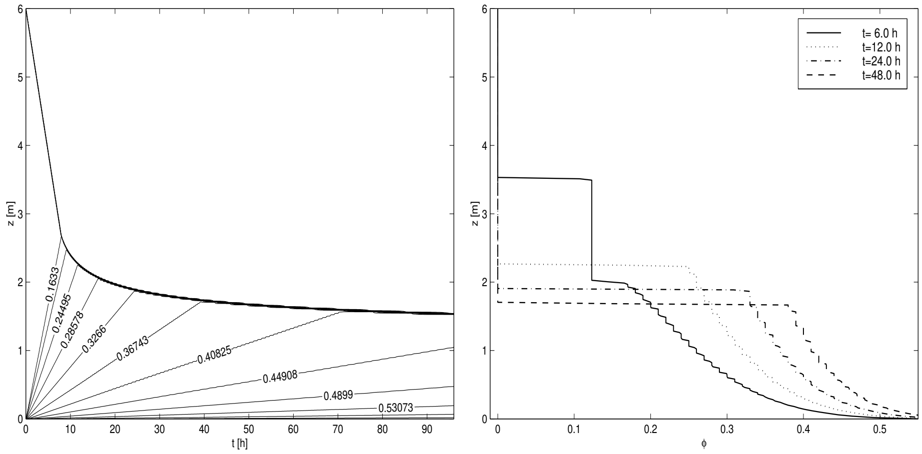

FIGURE 7. Settling plot (left) and concentration profiles (right) for batch settling of a flocculated suspension described by the Kynch theory and simulated by front tracking.

velocity is assumed to be constant and we set $q = -1.5 \times 10^{-5}$ [m/s]. The ICT will first be filled, then attain a steady state with discharge concentration 0.39, and finally be emptied by manipulating the feed flux density $f_{\mathrm{F}} = q(t)\phi_{\mathrm{L}}(t) + f_{\mathrm{bk}}(\phi_{\mathrm{L}}(t))$. Namely, we set

$$\phi_L(t) = \begin{cases} 0.06, & \text{for } 0 < t \leq 70000 \text{ [s]} \approx 0.81 \text{ [days]}, \\ 0.01077641, & \text{for } 70000 \text{ [s]} < t \leq 600000 \text{ [s]} \approx 6.94 \text{ [days]}, \\ 0, & \text{for } t > 600000 \text{ [s]}. \end{cases}$$

We simulated the process up to time $T = 10$ [days] using 8640 time steps on a 300 grid, corresponding to a CFL number of 2.8. Figure 8 shows the settling plot and some selected concentration profiles for this simulation.

5.3. **Transition Between Steady States.** To demonstrate that the three-step splitting method presented in §4.2 is equally suited for simulation of sedimentation with compression, we take the same Kynch batch flux density function $f_{\mathrm{bk}}(\phi)$ and the same effective stress function $\sigma_{\mathrm{e}}(\phi)$ as before and consider continuous sedimentation with piecewise constant average flow velocity $q(t)$ and feed flux $f_{\mathrm{F}}(t)$.

We start with a steady state, a stationary concentration profile, and then attain two new steady states by manipulating f_{F} and q appropriately. Steady states are obtained as stationary solutions of equation (5). It is assumed that a desired discharge concentration ϕ_{D} is prescribed. Then the discharge flux is $f_{\mathrm{D}} = q\phi_{\mathrm{D}}$. The requirement that at steady state the discharge flux must equal the feed flux, $f_{\mathrm{D}} = f_{\mathrm{F}}$, leads to an equation from which the concentration value ϕ_L at $z = L$ can be computed:

$$q\phi_L + f_{\mathrm{bk}}(\phi_L) = q\phi_{\mathrm{D}}. \tag{26}$$

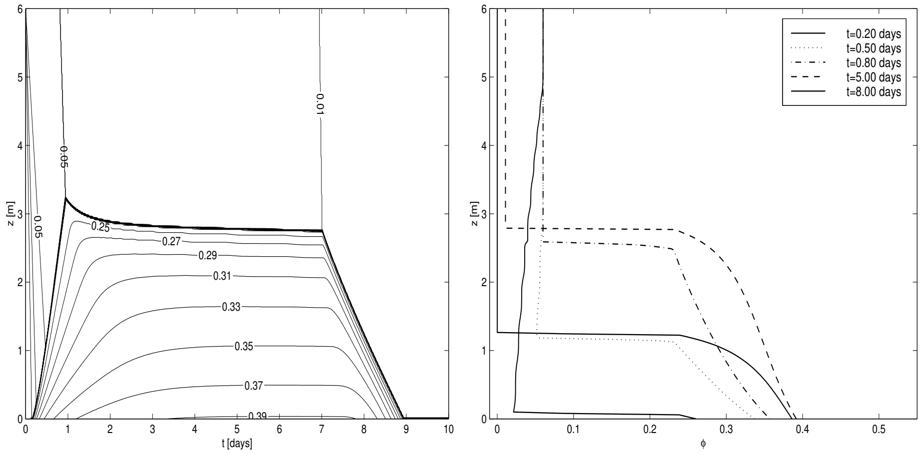

FIGURE 8. Settling plot (left) and concentration profiles (right) for filling and emptying of a continuous thickener simulated by operator splitting (20).

The sediment concentration profile is then calculated from

$$\frac{d\phi}{dz} = \frac{q\phi(z) + f_{\mathrm{bk}}(\phi(z)) - q\phi_{\mathrm{D}}}{a(\phi(z))}, \quad z > 0, \quad \phi(0) = \phi_{\mathrm{D}}. \tag{27}$$

The boundary value problem (27) is solved until the critical concentration is reached at a certain height z_{c} denoting the sediment level. Above this level, the concentration assumes the constant value ϕ_L calculated from (26). The choice of ϕ_{D} is subject to the requirement that the concentration increases downwards. See Bürger *et al.* [44] and Bürger and Concha [47] for details. Consider the three steady states with parameters given in Table 1.

i	$q^i\,[10^{-4}\,\mathrm{m/s}]$	ϕ_{D}^i	ϕ_L^i	$f_{\mathrm{F}}^i\,[10^{-4}\,\mathrm{m/s}]$	$z_{\mathrm{c}}\,[\mathrm{m}]$
1	-0.10	0.41	0.0072993552	-0.041	3.10
2	-0.15	0.38	0.0104589127	-0.057	1.77
3	-0.05	0.42	0.0036012260	-0.021	2.49

TABLE 1. Parameters of the steady states considered in Figure 9.

We now prescribe the steady state $\phi_1(z)$ as the initial concentration profile. After operating the ICT at this steady state for some time, we then change successively to the steady states $\phi_2(z)$ and $\phi_3(z)$. The changes in $\phi_L(t)$ and $q(t)$ will be described in detail now.

The ICT is operated at the steady state $\phi_1(z)$ for $0 < t \leq t_2 = 50000\,[\mathrm{s}]$. At $t = t_2$, we change the volume average velocity q to the next smaller value q^2. However, the value of the feed flux density should remain constant during this operation, therefore the boundary concentration value ϕ_L^1 has to be changed to a new value ϕ_L^{12}, which is calculated from the feed flux continuity condition

$$q^2\phi_L^{12} + f_{\mathrm{bk}}(\phi_L^{12}) = f_{\mathrm{F}}^1,$$

yielding $\phi_L^{12} = 0.0076397602$. The change from ϕ_L^1 to ϕ_L^{12} should be performed at such a time that the new value ϕ_L^{12} is present above the sediment level at $t = t_2$. The change propagates as a rarefaction wave into the vessel. This rarefaction wave is marked by $\mathcal{R}_1$ in Figure 9 b). We assume that the relevant speed is

$$\sigma_2 = q^1 + f'_{\mathrm{bk}}(\phi_L^{12}) = -5.0607 \times 10^{-4}\,[\mathrm{m/s}],$$

therefore the change from ϕ_L^1 to ϕ_L^{12} is performed at

$$t_1 = t_2 + \frac{L - z_{\mathrm{c}}^1}{\sigma_2} = 48222\,[\mathrm{s}] \approx 13.4\,[\mathrm{h}].$$

It should be noted that the feed flux does not remain precisely constant; it is different from f_{F}^1 in the small time interval $[t_1, t_2]$, during which we have

$$f_{\mathrm{F}} = f_{\mathrm{F}}^{12} = q^1\phi_L^{12} + f_{\mathrm{bk}}(\phi_L^{12}) = f_{\mathrm{F}}^1 + (q^1 - q^2)\phi_L^{12} = -0.04138 \times 10^{-4}\,[\mathrm{m/s}].$$

From Figure 9 e) it becomes apparent that for $t > t_2$, the actual solids discharge flux density $f_{\mathrm{D}}(t) = q^2\phi(0,t)$ is larger than the feed flux f_{F} prescribed. This leads to a slow emptying of the vessel and the sediment level falls at almost constant speed. It may therefore be estimated that it will have fallen to the height z_{c}^2 of the next target steady state by $t = 316560\,[\mathrm{s}] \approx 87.9\,[\mathrm{h}]$. At that time, the concentration value ϕ_L^2 corresponding to the new feed flux density f_{F}^2 should have propagated to the sediment level. Again, this change propagates downwards as a rarefaction wave (marked by $\mathcal{R}_2$ in Figure 9 b)). The relevant propagation velocity may be taken as

$$\sigma_4 = q^2 + f'_{\mathrm{bk}}(\phi_L^2) = -4.7746 \times 10^{-4}\,[\mathrm{m/s}],$$

hence we change ϕ_L again from ϕ_L^{12} to ϕ_L^2 at

$$t_3 = 316560\,[\mathrm{s}] + \frac{L - z_{\mathrm{c}}^2}{\sigma_4} = 311854\,[\mathrm{s}] \approx 86.6\,[\mathrm{h}].$$

For $t > t_3$, both the value of q and the feed flux f_{F} correspond to the steady state $\phi_2(z)$ given in Table 1. Although this value is not prescribed explicitly, we observe in Figures 9 d) and e) that both the discharge flux and the discharge concentration converge to the appropriate values pertaining to the target steady state $\phi_2(z)$. At $t_5 = 600000\,[\mathrm{s}] \approx 166.7\,[\mathrm{h}]$ we wish to change to the next steady state by changing q from q^2 to q^3. The feed flux above the sediment is assumed to remain constant. Therefore ϕ_L^2 is changed to the value $\phi_L^{23} = 0.0113417003$ which is calculated from

$$q^3\phi_L^{23} + f_{\mathrm{bk}}(\phi_L^{23}) = f_{\mathrm{F}}^2.$$

Again, the change from ϕ_L^2 to ϕ_L^{23} propagates as a rarefaction wave into the vessel (marked by $\mathcal{R}_3$ in Fig. 9 b)). The value ϕ_L^{23} propagates at speed

$$\sigma_6 = q^2 + f'_{\mathrm{bk}}(\phi_L^{23}) = -4.6338 \times 10^{-4}\,[\mathrm{m/s}],$$

hence the change is performed at

$$t_4 = t_5 + \frac{L - z_{\mathrm{c}}^2}{\sigma_6} = 595182\,[\mathrm{s}] \approx 165.3\,[\mathrm{h}].$$

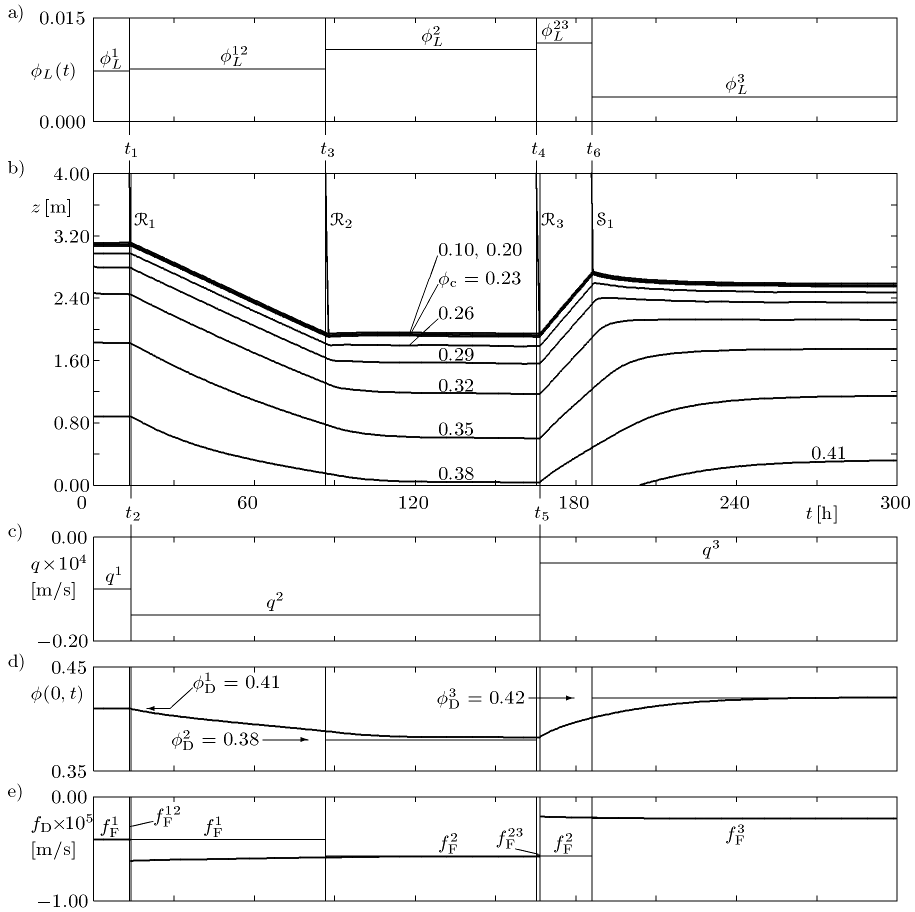

FIGURE 9. Simulation of transitions between three steady states in an ICT using the operator splitting method (25): a) prescribed values of ϕ_L, b) settling plot (the iso-concentration lines correspond to the annotated values), c) prescribed values of $q(t)$, d) the numerically calculated discharge concentration, together with the discharge concentrations of the target steady states, e) the numerically computed solids discharge flux, compared with prescribed values of the feed flux.

Similar to the change from ϕ_L^1 to ϕ_L^{12}, the feed flux assumes a value in the time interval $[t_4, t_5]$ which is slightly different from f_F^2; namely, there we have

$$f_F = f_F^{23} = q^2\phi_L^{23} + f_{bk}(\phi_L^{23}) = f_F^2 + (q^3 - q^2)\phi_L^{23} = -0.0559 \times 10^{-4}\,[\mathrm{m/s}].$$

After $t = t_5$, the feed flux exceeds the discharge flux in absolute value, as can be conceived from Fig. 9 e). This causes a rise of the sediment level, again taking place at apparently constant speed, and it will have attained the last desired level z_c^3 when $t = 672240\,[\mathrm{s}] \approx 186.7\,[\mathrm{h}]$. At that time, the last value of the feed flux f_F^3 should be valid above the sediment level. In contrast to the previous changes of ϕ_L, the change from ϕ_L^{23} to ϕ_L^3 propagates as a shock (marked by $\mathcal{S}_1$ in Fig. 9 b)) with the speed

$$\sigma_7 = q^3 + \frac{f_{\mathrm{bk}}(\phi_L^{23}) - f_{\mathrm{bk}}(\phi_L^3)}{\phi_L^{23} - \phi_L^3} = -5.1391 \times 10^{-4}\,[\mathrm{m/s}].$$

This discontinuity reaches the sediment level at the desired time if the change from ϕ_L^{23} to ϕ_L^3 is done at

$$t_7 = 672240\,[\mathrm{s}] + \frac{L - z_{\mathrm{c}}^3}{\sigma_7} = 669301\,[\mathrm{s}] \approx 185.9\,[\mathrm{h}].$$

After $t = t_7$, no more changes are made. Figures 9 b), d) and e) indicate convergence to the third steady state. The simulation is terminated after a simulated time of $T = 300\,[\mathrm{h}] = 1080000\,[\mathrm{s}]$.

6. Conclusion

An appealing feature of the phenomenological sedimentation model is that one single equation can be used to describe both sedimentation and consolidation processes, i.e., without having to model the suspension-sediment interface as a moving boundary, which would make a separate interface equation necessary. This view is different from the approaches taken by Philip and Smiles [48], Pane and Schiffman [49], Stamatakis and Tien [24], Shodja and Feldkamp [23] and, in the case of poydisperse suspensions, by Shih *et al.* [50].

In this paper, we have presented numerical methods that automatically reproduce the discontinuities inherent to solutions of the mixed hyperbolic-parabolic convection-diffusion problem modeling sedimentation-consolidation processes. In particular, we avoid an explicit moving sediment-suspension interface condition (as in Stamatakis and Tien [24]), which would have significantly complicated the development of numerical methods. In fact, it has been the main objective of this paper to demonstrate that the concept of hyperbolic-parabolic PDEs does not imply severe numerical problems as long as one employs conservative methods that obey a discrete entropy principle.

It is a well accepted practice to utilize conservative methods when solving numerically first order hyperbolic PDEs [12]–[15]. Shock waves are the solution features that demand conservative methods. A non-conservative method yields solutions with wrong shock strength, wrong shock speed, and thus wrong shock position. It is well known that if a conservative method converges, it does so to a weak solution of the conservation law. If the method also satisfies a discrete entropy principle, the converged solution is the physical weak solution. In the sedimentation model, the governing PDE is a nonlinear convection-diffusion equation of mixed hyperbolic-parabolic type; that is, for $\phi < \phi_{\mathrm{c}}$ the PDE degenerates into hyperbolic PDE provided by Kynch's theory of sedimentation, whereas for $\phi \geq \phi_{\mathrm{c}}$ it behaves like a second order parabolic PDE. Consequently, the numerical methods for the sedimentation should, of course, employ a conservative discretization of the first order flux term. Perhaps somewhat less obvious is that one should also utilize a conservative discretization of the second order diffusion term in the model. In fact, we have demonstrated numerically (see Example 3.1) that a non-conservative discretization of the second order term yields discontinuous solutions with wrong shock strength and wrong shock location, see also [19]. To further back up the use of conservative methods, it can be shown that that if a conservative method for the sedimentation model converges, it does so to a weak solution of the model. Moreover, if this method also satisfies a discrete entropy principle, then the converged solution is the physically correct solution, see [16]–[21].

We have presented numerical methods that are suitable for simulation the settling of flocculated suspensions. Both finite difference methods and methods based on operator splitting have been considered. The methods are all mathematically sound in the sense that they use a conservative discretization of both first and second order terms in the governing PDE, they have built in a discrete entropy principle, and thus produce physically correct solutions. For simulation purposes, we recommend the use of operator slitting methods based on optimal numerical methods for first order hyperbolic PDEs and a conservative finite difference discretization of the second order part of the model. One should note that if the chosen hyperbolic solver is a conservative method obeying a discrete entropy principle, it can be proved that the resulting operator splitting method is also a conservative method obeying a discrete entropy principle, see [16, 20]. The reason for choosing operator splitting methods over unsplit difference methods is partially that splitting methods are more efficient than unsplit methods.

We are well aware that only the most essential features of industrial thickeners can be cast into the concept of an ICT. In particular, phenomena occurring when the sediment should reach the feed level are not correctly predicted by this setup, see Lev *et al.* [51]. A better one-dimensional concept is that of a settler-clarifier unit, in which the feed is represented by a singular source term. This configuration has been intensively studied by Diehl [52, 53, 54] for the case of Kynch's theory and should also be considered for the phenomenological theory. A further possible application of the methods presented here could be the extension to a model for the settling of polydisperse suspensions (with particles of different sizes and densities) including compression effects, see Stamatakis and Tien [24]. Bürger *et al.* have already shown [55] that the Nessyahu and Tadmor [43] method can be successfully employed for the solution of the system of conservation laws arising from the kinematical theory of sedimentation of polydisperse suspensions.

Acknowledgement

KHK is grateful to the group of Prof. Dr.-Ing. W.L. Wendland at the Institute of Mathematics A, University of Stuttgart, for hospitality. The research of KHK was supported by the Applied Mathematics in Industrial Flow problems (AMIF) program of the European Science Foundation. Support by the Sonderforschungsbereich 404 at the University of Stuttgart is also acknowledged.

Nomenclature

Latin Letters.

$a(\phi)$	diffusion function
$A(\phi)$	primitive of the diffusion function
$f(\phi, t)$	solids flux density function

$f_{\mathrm{bk}}(\phi)$	Kynch batch flux density function
f_{D}	discharge flux
f_{F}	feed flux
f_{F}^1, f_{F}^2, f_{F}^3	values of f_{F} given in Table 1
f_{F}^{12}, f_{F}^{23}	values of f_{F} related to transitions between steady states
F	upwind flux
g	acceleration of gravity
$\mathcal{H}(t)$	solution operator of (19) or (22), depending on the context
L	settling column height/height of the surface source in an ICT
p_{e}	excess pore pressure
q	volume average velocity
q^1, q^2, q^3	values of q given in Table 1
$\mathcal{R}_1$, $\mathcal{R}_2$, $\mathcal{R}_3$	rarefaction waves drawn in Fig. 9
$s(\cdot,\cdot)$	limiter function used by the second order upwind method
$\mathcal{S}_1$	shock line drawn in Fig. 9
$\mathcal{S}^f(t)$	solution operator of (18)
$\mathcal{S}^{f_{\mathrm{bk}}}(t)$	solution operator of (24)
$\mathcal{S}^q(t)$	solution operator of (23)
t	time variable
$t_1,\dots,t_6$	control times, see §5.3
t_n	discrete time
T	endpoint of simulated time interval
v_{f}	fluid phase velocity
v_{s}	solids phase velocity
z	spatial variable
z_{c}	sediment height
z_{c}^1, z_{c}^2, z_{c}^3	values of z_{c} given in Table 1
z_j	grid point

Greek letters.

$\alpha(\phi)$	function relating the solid-fluid interaction force to $v_{\mathrm{s}} - v_{\mathrm{f}}$
Δz	spatial discretization parameter
Δt	temporal discretization parameter
$\Delta\varrho$	difference of solids and fluid mass densities
ϕ	volumetric solids concentration
ϕ_{c}	critical concentration value
ϕ_{D}	discharge concentration
ϕ_{D}^1, ϕ_{D}^2, ϕ_{D}^3	values of ϕ_{D} given in Table 1
$\phi_{\max}$	maximum solids concentration
$\phi_0(z)$	initial concentration distribution
$\phi_1(z)$, $\phi_2(z)$,$\phi_3(z)$	steady states considered in §5.3
ϕ_j^n	numerical approximation of ϕ

ϕ_L	prescribed concentration value at $z = L$
ϕ_L^1, ϕ_L^2, ϕ_L^3	values of ϕ_L given in Table 1
ϕ_L^{12}, ϕ_L^{23}	values of ϕ_L related to transitions between steady states
ϕ_j^{L}, ϕ_j^{R}	extrapolated values used by the second order upwind method
$\phi_{\Delta t}(z, t_n)$	operator splitting approximation of ϕ
ϱ_{f}	fluid density
ϱ_{s}	solids density
σ_2, σ_4, σ_6, σ_7	propagation velocities considered in §5.3
$\sigma_{\mathrm{e}}(\phi)$	effective solid stress function
τ	local temporal discretization parameter defined in (21)

References

[1] F. Concha and M.C. Bustos, in B.M. Moudgil and P. Somasundaran (eds.), Proceedings of the EF Conference on Flocculation, Sedimentation and Consolidation, Sea Island, GA, AIChE, New York 1986, p. 275.

[2] M.C. Bustos, F. Concha, R. Bürger and E.M. Tory, Sedimentation and Thickening: Phenomenological Foundation and Mathematical Theory, Kluwer Acedemic Publishers, Dordrecht, The Netherlands, to appear.

[3] F. Concha, M.C. Bustos and A. Barrientos, in E.M. Tory (ed.), Sedimentation of Small Particles in a Viscous Fluid, Computational Mechanics Publications, Southampton, UK, 1996, Chapter 3.

[4] G.J. Kynch, Trans. Farad. Soc. 48 (1952) 166.

[5] M.C. Bustos, F. Concha and W.L. Wendland, Math. Meth. Appl. Sci. 13 (1990) 1.

[6] F. Concha and M.C. Bustos, Int. J. Mineral Process. 34 (1992) 33.

[7] R. Bürger, S. Evje, and K.H. Karlsen, in preparation.

[8] R. Bürger and W.L. Wendland, Math. Meth. Appl. Sci. 21 (1998) 865.

[9] R. Bürger and W.L. Wendland, J. Math. Anal. Appl. 218 (1998) 207.

[10] M.C. Bustos and F. Concha, Math. Meth. Appl. Sci. 10 (1988) 245.

[11] C.A. Petty, Chem. Engrg. Sci. 30 (1975) 1451.

[12] E. Godlewski and P.-A. Raviart, Numerical Approximation of Hyperbolic Systems of Conservation Laws, Springer-Verlag, New York, 1996.

[13] D. Kröner, Numerical schemes for conservation laws, John Wiley & Sons Ltd., Chichester, UK, 1997.

[14] R.J. LeVeque, Numerical methods for conservation laws, Birkhäuser Verlag, Basel, Switzerland, 2nd ed., 1992.

[15] E.F. Toro, Riemann Solvers and Numerical Methods for Fluid Dynamics, Springer-Verlag, Berlin 1997.

[16] R. Bürger, S. Evje and K.H. Karlsen, in preparation.

[17] S. Evje and K.H. Karlsen, in preparation.

[18] S. Evje and K.H. Karlsen, submitted to Numer. Math.

[19] S. Evje and K.H. Karlsen, to appear in SIAM J. Numer. Anal.

[20] S. Evje and K.H. Karlsen, to appear in Numer. Math.

[21] S. Evje and K.H. Karlsen, to appear in Proc. 7th Internat. Conf. Hyperbolic Problems, Zürich 1998.

[22] M.S. Espedal and K.H. Karlsen, in A. Fasano and H. van Duijn (eds.), Filtration in Porous Media and Industrial Applications, Lecture Notes in Mathematics, Springer-Verlag, to appear.

[23] H.M. Shodja and J.R. Feldkamp, Int. J. Num. Anal. Meth. Geosci. 17 (1993) 753.

[24] K. Stamatakis and C. Tien, Powder technol. 72 (1992) 227.

[25] P.T. Shannon and E.M. Tory, Trans. SME 235 (1966) 375.

[26] F. Concha and R. Bürger, in E.F. Toro and J.F. Clarke (eds.), Numerical Methods for Wave Propagation, Kluwer Academic Publishers, Dordrecht, The Netherlands, 1998, p. 173.
[27] R. Bürger, submitted to the UEF Conf. on Solid-Liquid Separation Systems, Kahuku, Oahu, HI, USA, 1999.
[28] M.D. Green, M. Eberl and K.A. Landman, AIChE J. 42 (1996) 2308.
[29] K.A. Landman and L.R. White, Adv. Colloid Interf. Sci. 51 (1994) 175.
[30] M.C. Bustos, F. Paiva and W.L. Wendland, Math. Meth. Appl. Sci. 12 (1990) 533.
[31] K.H. Karlsen and N.H. Risebro, to appear in SIAM J. Numer. Anal.
[32] K.H. Karlsen, K. Brusdal, H. K. Dahle, S. Evje, and K.-A. Lie, Comp. Meth. Appl. Mech. Engrg. 167 (1998), 239-260.
[33] K.H. Karlsen and K.-A. Lie, to appear in IMA J Numer. Anal.
[34] H. Holden and N. H. Risebro, Front Tracking for Conservation Laws, Lecture Notes, Department of Mathematics, Norwegian University of Science and Technology, Trondheim 1997.
[35] C.M. Dafermos, J. Math. Anal Appl. 38 (1972).
[36] K.-A. Lie, Front Tracking and Operator Splitting for Convection Dominated Problems, Dr. ing. thesis, NTNU Trondheim, Norway, 1998.
[37] H. Holden and L. Holden, in S. Albeverio, J. E. Fenstad, H. Holden, and T. Lindstrøm, editors, Ideas and Methods in Mathematics and Physics, Cambridge University Press, Cambridge, UK, 1988 p. 480.
[38] H. Holden, L. Holden, and R. Høegh-Krohn, Comp. Math. Appl. 15 (1988) 595.
[39] N.H. Risebro, Proc. Amer. Math. Soc. 117 (1993) 1125.
[40] K.-A. Lie, Preprint Mathematics No. 16, Norwegian University of Science and Technology, Trondheim, Norway, 1997.
[41] K.H. Karlsen, K.-A. Lie, and N.H. Risebro, to appear in Proc. 7th Int. Conf. Hyperbolic Problems, Zürich 1998.
[42] R. Bürger and W.L. Wendland, to appear in Proc. 4th Int. Conf. on Numerical Methods and Applications, Sofia, Bulgaria, 1998, World Scientific, Singapore.
[43] H. Nessyahu and E. Tadmor, J. Comp. Phys. 87 (1990) 408.
[44] R. Bürger, M.C. Bustos and F. Concha, Int. J. Mineral Process. 54 (1999) 267.
[45] J.F. Richardson and W.N. Zaki, Trans. Inst. Chem. Engrs. (London) 32 (1954) 35.
[46] R. Becker, Espesamiento Continuo, Diseño y Simulación de Espesadores, Engineering Thesis, Dept. of Metallurgical Engineering, University of Concepción, Chile, 1982.
[47] R. Bürger and F. Concha, Int. J. Multiphase Flow 24 (1998) 1005.
[48] J.R. Philip and D.E. Smiles, Adv. Colloid Interf. Sci. 17 (1982) 83.
[49] V. Pane and R.L. Schiffman, Géotechnique 35 (1985) 69.
[50] Y.T. Shih, D. Gidaspow and D.T. Wasan, Powder Technol. 50 (1987) 201.
[51] O. Lev, E. Rubin and M. Sheintuch, AIChE J. 32 (1986) 1516.
[52] S. Diehl, SIAM J. Math. Anal. 26 (1995) 1425.
[53] S. Diehl, SIAM J. Appl. Math. 56 (1996) 388.
[54] S. Diehl, SIAM J. Appl. Math. 57 (1997) 991.
[55] R. Bürger, F. Concha, K.K. Fjelde and K.H. Karlsen, Preprint 99/02, Sonderforschungsbereich 404, University of Stuttgart, submitted to Powder Technol.